Waves in Guinness

Marguerite Robinson,[1] A. C. Fowler,[1,2] A. J. Alexander,[3] and S. B. G. O'Brien[1,a)]
[1]*Department of Mathematics and Statistics, University of Limerick, Limerick, Republic of Ireland*
[2]*Mathematical Institute, Oxford University, 24-29 St. Giles', Oxford OX1 3LB, United Kingdom*
[3]*School of Chemistry, University of Edinburgh, Edinburgh EH9 3JJ, Scotland*

We describe a simple model of a bubbly two-phase flow which is able to explain why waves propagate downward when a pint of Guinness is poured, and also how the waves are generated. Our theory involves a physically based regularization of the basic equations of the two-phase flow, using interphasic pressure difference and virtual mass terms, together with bulk or eddy viscosity terms. We show that waves can occur through an instability analogous to that which forms roll waves in inclined fluid flows, and we provide a description of the form of these waves, and compare them to observations. Our theory provides a platform for the description of waves in more general bubbly two-phase flows, and the way in which the flow breaks down to form slug flow. © 2008 American Institute of Physics. [DOI: 10.1063/1.2929369]

I. INTRODUCTION

Two-phase flows of a gas-liquid mixture have many important applications in industry, for example, in heat exchangers, reactor cooling systems, and oil extraction. The particular case of gas-liquid flows in a vertical pipe is characterized by a number of different flow regimes. Two of the principal flow regimes are those of bubbly flow, in which small gas bubbles are dispersed throughout a continuous liquid phase, and slug flow, where slugs of liquid are separated by large gas bubbles whose width approaches the diameter of the pipe.

It is well established that a bubbly flow in a vertical pipe may undergo a transition to the slug flow regime and this transition is characterized by wave formation in the bubbly flow.[1–3] The classical explanation for these waves lies in the kinematic wave theory developed in Refs. 4–6, based (in terms of a two-phase flow theory) on a suitable drift flux model. The same types of waves occur in the flow of suspensions, sedimentation, and in traffic flows (see, for example, Refs. 7–10) and can be explained in similar ways. What is less clear is why such waves should form in the first place. A natural idea is that the uniform state with constant void fraction (the volume fraction of bubbles) should be unstable to void fraction disturbances. In fact, the breakdown of bubbly flow to slug flow as the void fraction increases is thought to result from instability of the uniform flow, leading to voidage waves or concentration waves in the bubbly flow, and such an instability is thought to herald the regime transition to slug or churn flow as well as the analogous transition to bubbly flow in fluidized beds.[11] Thus, an understanding of the bubble-to-slug regime transition requires knowledge of voidage waves and their onset.

An issue of some concern relating to two-phase flow models is the occurrence of complex characteristics resulting in an improperly posed initial-boundary-value problem.[12,13] Considerable attention has been paid in resolving this issue,

whereby the inclusion of more physically realistic terms can render the equations well-posed for finite values of the void fraction. In the context of bubbly two-phase flows, it is suggested in Ref. 14 that the breakdown of bubbly flow and the subsequent transition to slug flow was associated with a coalescence of the characteristic speeds (and their subsequently becoming complex) at a critical value of the void fraction. While such an occurrence undoubtedly heralds instability, it does so in an ill-posed way since the resulting instability occurs at all wave numbers.[15] It is suggested in Ref. 16 that the inclusion of higher derivative terms could remedy this and such a model is considered in Ref. 12. Thus, it appears that the issue of instability is inextricably linked to the vexed question of the proper formulation of the two-phase flow equations. In turn, this is associated with the proper prescription of boundary conditions for the flow, a topic which is fundamental but which has been largely ignored.

Laboratory experiments of these gas-liquid flows are mostly restricted to simple air/water systems, in which the waves can be remotely sensed but they are not easily seen.[1,3] Industrially important flows, such as that of oil/gas flow in a borehole of an oil well, can also only be sensed remotely. It is therefore particularly attractive to find an experimental realization of the two-phase flow waves in which the waves are easily seen, and such a realization occurs in the simple case of gas-liquid flow in a poured glass of Guinness. For this reason, in the remainder of this paper, we focus on this particularly common flow.

When a pint of Guinness or other comparable beer is poured and allowed to settle, waves can be seen in the resulting bubbly liquid, propagating downward despite the fact that the bubbles are buoyant. It is now known (see Ref. 17) that the waves are embedded in a convective circulatory flow which descends near the wall and rises at the center. A pint of Guinness can be considered a mixture of a viscous (black) liquid and (buoyant) nitrogen bubbles. During the settling process, the "head" of the pint is gradually formed via the accumulation of the bubbles at the upper surface of the black

a)Electronic mail: stephen.obrien@ul.ie.

FIG. 1. (Color online) Waves in the Guinness and roll waves on a roadway in Craggaunowen, County Clare, Ireland. In the Guinness, the waves propagate downward and are superimposed on a circulatory motion whose origin appears to be due to buoyancy induced convection itself due to a lateral variation in void fraction. Photograph courtesy of Michael Manga ["Waves of bubbles in basaltic magmas and lavas," J. Geophys. Res. **101**, 457 (1996) (Ref. 18)].

liquid and it is the contrast between the creamy bubble foam at the top and the black liquid beneath which gives the pint of Guinness its characteristic black/white appearance. Here, we are concerned with the early stages of the settling process when the glass is full of an approximately uniform light brown mixture of liquid and bubbles. The experienced observer of this phenomenon will note the occurrence of a periodic train of waves, manifested as a series of irregular horizontal dark lines appearing to flow downward in the brown mixture. In this paper, we will develop a theory for these waves and we will show that in a mathematical sense, they are analogous to, and represent a generalization of the roll waves in a fluid film, which can commonly be seen following heavy rainfall in the water films flowing down an inclined laneway (Fig. 1).

Our purpose in this paper, therefore, is to examine the onset and propagation of waves in bubbly flow, in the context of a properly constituted two-phase flow model. We introduce our basic model for two-phase flows in Sec. II. (The derivation of the model is contained in Appendix A.) In Sec. III, we analyze a simplified model and show that the basic steady flow is linearly unstable and the instability always occurs before the onset of complex characteristics, which we suppose signals a transition to slug flow. As such, wave formation in the bubbly flow can be viewed as a precursor to a regime transition. We then further analyze the simplified (hyperbolic) model for the development of periodic wave trains and we compare the results to the numerical solutions (Sec. IV) of the full evolution equations including a smoothing eddy viscosity term. A discussion follows in Sec. V and the conclusions are in Sec. VI.

II. THE MATHEMATICAL MODEL

We consider the specific example of wave generation in a bubbly flow and we focus on the specific form of waves seen in the initial pouring of a glass of the Guinness. We use a continuum model with the relevant continuum variable α being the void fraction, i.e., the ratio of gas volume to the total volume of the gas/liquid mixture (so $\alpha=0$ corresponds to pure liquid).

We propose a model based on the use of averaged equations. As exhaustively described by Refs. 19–21 and many other authors, there are a variety of different conceptual methodologies by which one can average. Generally, these lead to similar forms of the averaged equations, depending on one's assumptions about the small scale flow. A popular choice is the ensemble average, in which one averages the equations over many different realizations. Alternatively, one may time average, where the small scale fluctuation time scale is much smaller than the macroscopic (convective) time scale; or one may space average, where one assumes that the microscopic space scale (here, the bubble diameter) is much less than the macroscopic length scale. We do not dwell on the averaging procedure but note that the spatial averaging procedure is implicitly assumed in the discussion below.

We leave the details of the derivation of the equations appropriate for waves in Guinness to Appendix A, where we rehearse the basic ill-posedness of the one-dimensional two-phase flow equations and discuss the setting of correctly posed boundary value problems, and the consequent interpretation of flow regime diagrams in terms of such problems. We further suggest a physically based constitutive law for the interphasic pressures, which is closely related to a model introduced in Ref. 22 in the context of fluidized beds and used in Ref. 23 to study void fraction waves in bubbly flow (see also Ref. 24). A related model is considered in Ref. 25. We show that this constitutive law acts as a bulk viscosity and produces a diffusive term in the liquid momentum equation.

The full model with boundary conditions is discussed in Appendix A and is given by

$$\alpha_t + (\alpha v)_x = 0, \tag{2.1a}$$

$$-\alpha_t + [(1-\alpha)u]_x = 0, \tag{2.1b}$$

$$\rho_l(1-\alpha)(u_t + uu_x) = -(1-\alpha)\frac{\partial p_l}{\partial x} + F_{gi} - F_{lw} + (p_l - p_g)\frac{\partial \alpha}{\partial x}$$
$$+ \alpha\rho_l C_{VM}[v_t + vv_x - (u_t + uu_x)]$$
$$- (1-\alpha)\rho_l g + \frac{\partial}{\partial x}[\eta(1-\alpha)u_x], \tag{2.1c}$$

$$\rho_g\alpha(v_t + vv_x) = -\alpha\frac{\partial p_g}{\partial x} - F_{gi} - \alpha\rho_g g$$
$$- \alpha\rho_l C_{VM}[v_t + vv_x - (u_t + uu_x)], \tag{2.1d}$$

where we choose the constitutive law for interfacial pressure difference as

$$p_g - p_l = -H\rho_l(v-u)^2. \tag{2.2}$$

A detailed discussion of appropriate choices for the coefficients is given in Ref. 26. The variables are the void fraction α, the averaged gas and liquid velocities v and u, and the gas and liquid pressures p_g and p_l; x denotes the along axis distance, and F_{gi} and F_{lw} are the frictional resistance exerted on the gas by the liquid (at the gas-liquid interface) and the wall friction exerted on the liquid, respectively. We note that the last four terms in Eq. (2.1c) represent the interphasic pressure, a virtual mass term, gravity, and an eddy viscosity regularizing term, respectively, the last two terms in Eq. (2.1d)

represent gravity and virtual mass effects, respectively. We follow Refs. 23, 26, and 27 by including virtual mass effects as well as the interfacial pressure difference Δp_{li} and the eddy/bulk viscosity. For the purposes of simplicity and didacticism, we make simple choices,

$$C_{VM} = \tfrac{1}{2}, \quad H = \tfrac{1}{4}, \tag{2.3}$$

which are appropriate for isolated spherical bubbles. For the phenomenon under consideration, that of the propagation of waves in an essentially quiescent medium, we set $F_{lw} = 0$ and choose

$$F_{gi} = \frac{\mu D(\alpha)(v - u)}{a^2}, \tag{2.4}$$

corresponding to the laminar drag past bubbles of radius a, where μ is the liquid dynamic (laminar) viscosity. (In general, the eddy or bulk viscosity η will be larger than this.) For the Stokes drag as $\alpha \to 0$, we would have $D \approx 3\alpha$, while at large α, where Darcy's law might be more appropriate, the choice of $D = 180\alpha^2/(1-\alpha)$ corresponds to the Carman–Kozeny law.[28] For more violent flows, a better choice would have $F_{gi} \propto (v - u)^2$.

A. Nondimensionalization and simplification

If the liquid viscosity is μ, we define the dimensionless bulk viscosity

$$\eta^* = \frac{\eta}{\mu}, \tag{2.5}$$

in general, this will depend on α. For example, one possibility is

$$\eta^* \approx \frac{4}{3\alpha}, \tag{2.6}$$

neglecting gas viscosity, as demonstrated in Eq. (A19) of Appendix A 3. Suitable velocity, length, and time scales are given by

$$u_0 = \frac{a^2 g}{\nu_l}, \quad l = \frac{u_0^2}{g} = \frac{a^4 g}{\nu_l^2}, \quad t_0 = \frac{l}{u_0} = \frac{a^2}{\nu_l}, \tag{2.7}$$

where a is bubble radius and $\nu_l = \mu/\rho_l$ is the liquid kinematic viscosity. We nondimensionalize the equations by scaling

$$x \sim l, \quad u, \quad v \sim u_0, \quad p_l, \quad p_g \sim \rho_l u_0^2, \quad t \sim t_0. \tag{2.8}$$

The dimensionless forms of the mass conservation equations have the same form and the dimensionless momentum equations take the form

$$(1-\alpha)(u_t + uu_x) = -(1-\alpha)\frac{\partial p_l}{\partial x} + (p_l - p_g)\frac{\partial \alpha}{\partial x}$$
$$+ \alpha C_{VM}[v_t + vv_x - (u_t + uu_x)]$$
$$- [1 - \alpha - D(v - u)]$$
$$+ \varepsilon \frac{\partial}{\partial x}[\eta^*(1-\alpha)u_x], \tag{2.9}$$

$$\delta\alpha(v_t + vv_x) = -\alpha\frac{\partial p_g}{\partial x} - [\delta\alpha + D(v - u)]$$
$$- \alpha C_{VM}[v_t + vv_x - (u_t + uu_x)],$$

where

$$\varepsilon = \frac{a^2}{l^2} = \frac{\nu_l^4}{g^2 a^6}, \quad \delta = \frac{\rho_g}{\rho_l}. \tag{2.10}$$

With typical estimates for Guinness of $a \sim 0.06$ mm, $\nu_l \sim 2 \times 10^{-6}$ m^2 s^{-1}, $g \sim 10$ m s^{-2}, we have $l \sim 0.03$ mm, $\varepsilon \sim 2$, and the diffusion term is not so small. Worse, the length scale is smaller than the bubble radius. In this paper, we will consider a continuum model which formally requires $l \gg a$, and thus, $\varepsilon \ll 1$, but recognize that this may not be true in practice; to some extent, the problem is a cosmetic one, insofar as (for example) the large values of the coefficients g_i in the dimensionless model below suggest a larger length scale. The observations that motivate our study (wavelength some hundred times greater than bubble radius) support this viewpoint. With $\rho_l \sim 10^3$ kg m^{-3}, $\rho_g \sim 1$ kg m^{-3}, the parameter $\delta \sim 10^{-3}$ is also small.

Adding the two mass conservation equations, we have

$$\alpha v + (1-\alpha)u = j, \tag{2.11}$$

where the total volume flux j is constant. This allows us to write $v = v(\alpha, u)$. We set $\delta = 0$, thus neglecting the gas acceleration terms. Eliminating the pressure derivative terms in the momentum equations, we can write the model as two equations for α and u,

$$-\alpha_t + [(1-\alpha)u]_x = 0,$$

$$g_1 u_t + [g_1 j + g_2(u - j)]u_x - g_3(u - j)^2 \alpha_x$$
$$= -R + \frac{\varepsilon}{(1-\alpha)}[\eta^*(1-\alpha)u_x]_x, \tag{2.12}$$

where

$$R = 1 + \frac{D(\alpha)(u - j)}{\alpha^2(1-\alpha)}, \tag{2.13}$$

and

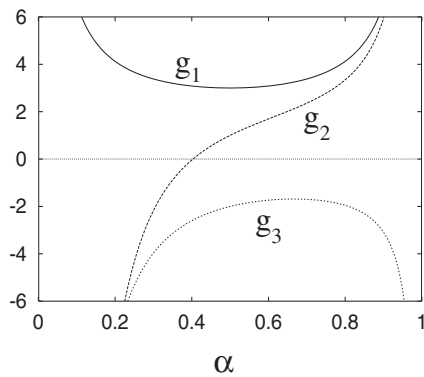FIG. 2. The coefficients g_1, g_2, and g_3 as functions of α for $C_{\mathrm{VM}} = \frac{1}{2}$, and $H = \frac{1}{4}$.

$$g_1 = 1 + \frac{C_{\mathrm{VM}}}{\alpha(1-\alpha)},$$

$$g_2 = 1 + \frac{2H}{\alpha^2} + \frac{C_{\mathrm{VM}}(3\alpha - 2)}{\alpha^2(1-\alpha)}, \qquad (2.14)$$

$$g_3 = -\left[\frac{C_{\mathrm{VM}} - H(2-\alpha)}{\alpha^3(1-\alpha)}\right].$$

The functions $g_1(\alpha)$, $g_2(\alpha)$, and $g_3(\alpha)$ are portrayed in Fig. 2. For the relevant values of $\alpha < 0.3$, we see that $g_1 > 0$, $g_2 < 0$, and $g_3 < 0$.

It is convenient to define

$$x = -\xi, \quad u = -w, \quad A = 1 - \alpha \qquad (2.15)$$

and we switch attention to the liquid fraction A ($A = 1$ corresponds to pure liquid). Note that g_1, g_2, and g_3 all become singular as $A \to 0$. Note also that the coordinate ξ points downward and that $w > 0$ corresponds to liquid downflow. The dimensionless equations are then

$$A_t + (Aw)_\xi = 0,$$

$$g_1 w_t + [g_2(w+j) - g_1 j] w_\xi + g_3(w+j)^2 A_\xi \qquad (2.16)$$

$$= R(A, w+j) + \frac{\varepsilon}{A}\frac{\partial}{\partial \xi}\left(\eta^* A \frac{\partial w}{\partial \xi}\right),$$

where

$$R(A, w) = 1 - \frac{w}{W(A)}, \qquad (2.17)$$

and we have written [with $D(A) = 3(1-A)$]

$$W(A) = \frac{(1-A)^2 A}{3(1-A)}. \qquad (2.18)$$

It is not difficult to show that under the transformation

$$w + j = w_0, \quad \xi + jt = X, \qquad (2.19)$$

the equations for $A(X,t)$ and $w_0(X,t)$ are precisely those above with the net volume flux $j = 0$. This is not surprising, indicating the Galilean invariance of the system. Conse-

quently, a solution $A(X,t)$, $w_0(X,t)$ when $j = 0$ yields solutions for nonzero j, in which

$$w(\xi, t) = w_0(\xi + jt, t) - j. \qquad (2.20)$$

In particular, traveling wave solutions of speed c_0 when $j = 0$ correspond to traveling waves when $j \neq 0$ of speed

$$c = c_0 - j. \qquad (2.21)$$

Because of this, it suffices to analyze the equations with $j = 0$ and these take the form

$$A_t + (Aw)_\xi = 0, \qquad (2.22a)$$

$$g_1 w_t + g_2 w w_\xi + g_3 w^2 A_\xi = R(A, w) + \frac{\varepsilon}{A}\frac{\partial}{\partial \xi}\left(\eta^* A \frac{\partial w}{\partial \xi}\right). \qquad (2.22b)$$

In particular, we wish to investigate the stability of the base steady flow $A = A^*$, $w = w^*$ representing essentially a steady state of constant velocity and volume fraction.

III. THE REDUCED MODEL ($\varepsilon = 0$)

In this section, we analyze Eq. (2.22) in the case when $\varepsilon = 0$.

A. Linear stability

If $\varepsilon = 0$, the characteristics $d\xi/d\tau = \lambda$ of Eq. (2.22) satisfy

$$\lambda = \frac{w}{2g_1}\{(g_1 + g_2) \pm [(g_1 - g_2)^2 + 4g_1 g_3 A]^{1/2}\}, \qquad (3.1)$$

and are real and distinct if the discriminant is positive. The basic case where $C_{\mathrm{VM}} = H = 0$ corresponds to $g_1 = g_2 = 1$, $g_3 = 0$, and the characteristic speeds are equal. As we discuss in Appendix A, the model with the Cauchy data is ill posed. When $C_{\mathrm{VM}} = \frac{1}{2}$ and $H = \frac{1}{4}$, then

$$g_1 - g_2 = \frac{1}{2(1-A)^2}, \quad 4g_1 g_3 A = -\frac{\left(A - A^2 + \frac{1}{2}\right)}{(1-A)^3 A}, \qquad (3.2)$$

and the characteristics are real and distinct if $A \gtrsim 0.735$ ($\alpha \lesssim 0.265$), as shown by Ref. 14. With $g_1 > g_2$ and $g_3 < 0$, the criterion for real characteristics can be written symbolically as

$$g_1 - g_2 > 2(g_1 |g_3| A)^{1/2}. \qquad (3.3)$$

(If $g_3 > 0$, the characteristics are always real.)

Equation (2.22) (neglecting the ε term) is comparable to the St. Venant equations which describe river flow,[28] and this analogy has been pointed out previously, if not in such a specific way.[24] The eddy viscosity term was discussed in the context of roll waves in Ref. 29. In that case, $g_1 = g_2 = F^2$, where F is the Froude number, $R = 1 - w^2/A$ for Chézy's law, and the crucial term $g_3 w^2 = 1$. The system is always hyperbolic since $g_3 > 0$ and the waves propagate in both directions if $F < 1$, and are exponentially decreasing in time. If $1 < F < 2$, then stable waves exist but both propagate in the same (downstream, toward $\xi = \infty$, i.e., downward) direction. Finally, if $F > 2$, then one of the downstream waves grows unstably and *roll waves* are formed. These waves are dis-
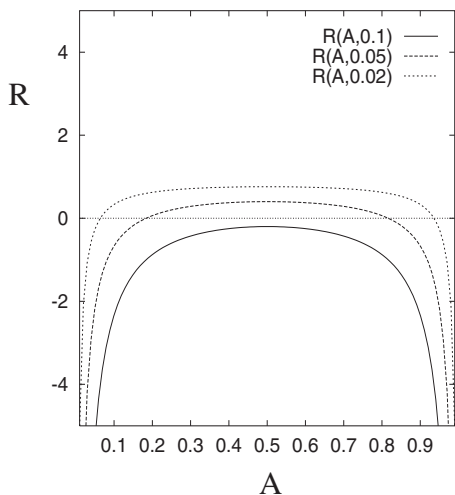
FIG. 3. Typical examples of $R(A, w)$ for R given by Eq. (2.17), with $D = 3\alpha$, $\alpha = 1 - A$.

cussed in Ref. 30 and have been analyzed in Ref. 31: they consist of a periodic sequence of shock waves. A more recent study is that of Ref. 32.

For the bubbly flow equation (2.22), we can reasonably take R as a concave in A, with R tending to $-\infty$ as $A \to 1$ or $A \to 0$ (see Fig. 3). An equilibrium exists at the uniform state (A^*, w^*) when $R(A^*, w^*) = 0$, and this determines w^* in terms of A^*. Let us assume that the drag law is $D \approx 3\alpha$; this is valid for $\alpha \to 0$ but we can in fact use it as a reasonable approximation for most values of α. Then, $W(A)$ in Eq. (2.18) is concave, $W(0) = W(1) = 0$ and

$$W(A) \approx \frac{A(1-A)}{3}. \tag{3.4}$$

Now, since $W(A)$ is quadratic in A, there are in fact two equilibria, one with $R_A > 0$ and $A^* < \frac{1}{2}$ and the other with $R_A < 0$ and $A^* > \frac{1}{2}$ (assuming the liquid velocity is positive, corresponding to downflow). For the particular choices $C_{VM} = \frac{1}{2}$ and $H = \frac{1}{4}$, we require $A > 0.735$ for real characteristics, and thus we focus on the equilibrium point with $R_A < 0$. We also have $R_w < 0$ and $g_3 < 0$. A straightforward linear instability analysis then shows that the uniform state is unstable if

$$g_1 - g_2 < \frac{g_1 A^* |R_A|}{|R_w| w^*} + \frac{|g_3||R_w| w^*}{|R_A|}, \tag{3.5}$$

or equivalently,

$$\begin{aligned} g_1 - g_2 &- 2(g_1 g_3 A^*)^{1/2} \\ &< \left[\left(\frac{g_1 A^* |R_A|}{|R_w| w^*} \right)^{1/2} - \left(\frac{|g_3||R_w| w^*}{|R_A|} \right)^{1/2} \right]^2, \end{aligned} \tag{3.6}$$

which shows, in comparison with Eq. (3.3) that the uniform state always becomes unstable *before* the characteristics become complex (i.e., we can ignore the latter in the context of the stability analysis). With $C_{VM} = 2H = \frac{1}{2}$ the uniform state (with $R_A < 0$) is unstable for all values of $A \geq 0$, if we assume Eq. (3.4) to be valid.

Linear theory seeks solutions of the form $A - A^* \propto \exp(ik\xi + \sigma t)$. Writing this in the equivalent form $A - A^* \propto e^{ik(\xi - c_L t) + \sigma_R t}$ demonstrates that the associated wave speed satisfies $c_L = -\sigma_I / k$. At the point of instability, corresponding to equality in Eq. (3.5) the unstable wave speed is

$$c_L = w^* - \frac{A^* |R_A|}{|R_w|}. \tag{3.7}$$

Since $w^* = W(A^*)$, we have

$$c_L = W(A^*) - A^* |W'(A^*)|, \tag{3.8}$$

and thus Eq. (3.4) implies

$$c_L \approx \frac{A^*}{3}(2 - 3A^*), \tag{3.9}$$

and the waves move in the negative ξ direction, i.e., *upward*, providing $A > \frac{2}{3}$. The upward motion of the waves is the result of analyzing Eq. (2.22) with $j = 0$, however, the actual wave speed will satisfy Eq. (2.21) (with $c_0 = c_L$), as discussed following Eq. (2.19).

B. Finite amplitude waves

If the uniform state $(A = A^*, w = w^*)$ of our fundamental equation set (2.22) is unstable to the formation of growing travelling waves, the question arises as to how such disturbances evolve.[23,33] In the spirit of kinematic wave theory, we attempt to find approximate travelling wave solutions of Eq. (2.22) with $\varepsilon = 0$. Later, we compare our results to the numerical solutions of the full equations (Sec. IV) for $\varepsilon \ll 1$. The normal precepts of nonlinear stability theory suggest the existence of finite amplitude periodic traveling waves but smooth solutions of this type cannot exist, for the following reason. If we seek solutions of the form

$$A = A(z), \quad w = w(z), \quad z = \xi - c\tau, \tag{3.10}$$

where c is to be determined, then there is a first integral

$$-cA + Aw = K, \tag{3.11}$$

and consequent substitution into Eq. (2.22b) yields a first order equation for A (or w). Such an equation cannot have periodic solutions.

The resolution of this quandary lies in the fact that the equations (with $\varepsilon = 0$) are hyperbolic. In general, we expect that isolated disturbances will evolve into propagating waves with a shock at one end and an expansion fan at the other (compare the discussion in Ref. 20, p. 284). Periodic disturbances may be expected to form periodic waves with a shock at one end, analogously to the formation of periodic shock waves in rivers.[31,34]

We therefore suppose that the solution for A takes the form of a function defined in $0 < z < L$, repeated periodically with period L (the wavelength), with $A = A_0$ at $z = 0$ and $A = A_L$ at $z = L$. With Eq. (3.11), the equation for A can be written as

$$J(A)A' = B(A), \tag{3.12}$$

where

$$J(A) = [(g_1 - g_2)cA - g_2K]K - |g_3|A(K + Ac)^2,$$

$$B(A) = A^2\left[A - \frac{K + Ac}{W(A)}\right].$$

(3.13)

The parameters c, K, L, A_0, and A_L are unknown. The integration of Eq. (3.12) from 0 to L determines L in terms of the other unknowns, thus,

$$L = \int_{A_0}^{A_L} \frac{J(A)dA}{B(A)}.$$

(3.14)

We now consider how the other unknown constants are to be found. In this, we follow Ref. 31 with one modification associated with the momentum balance.

1. Finite amplitude wave solutions

In Appendix B, we carry out a shock layer analysis in which we derive a momentum jump condition across the layer at $z=0$, L for the case $\varepsilon=0$ resulting in an expression for the shock speed

$$c = \frac{\left(w^2\left\{A\left[1 + \frac{H}{(1-A)^2}\right] - \frac{1}{2}C_{VM}\left[\frac{A^2}{(1-A)^2} - 1\right]\right\}\right)\Big|_{A_0}^{A_L} + \int_{A_0}^{A_L}\frac{AwJ(A)dA}{W(A)B(A)}}{\left[w\left(\frac{C_{VM}}{1-A} + A\right)\right]_{A_0}^{A_L}}.$$

(3.15)

Following the well established procedures from gas dynamics, we further examine the shock structure in Appendix B by performing a local analysis of Eq. (2.22) in the vicinity of a moving shock in the limit as $\varepsilon \to 0$ and this leads to Eqs. (B14) and (B15):

$$\int_{A_0}^{A_L} \frac{J(A)}{A^2}dA = 0,$$

(3.16)

$$\bar{A}[W(\bar{A}) - c] = K, \quad J(\bar{A}) = 0,$$

(3.17)

where $J(A)$ is defined in Eq. (3.13), $W(A) = A(1-A)/3$ and $\bar{A}$ is a particular value of A between A_0 and A_L defined by Eq. (3.17).

Interestingly, we find that the momentum jump and shock speed conditions are independent and, in fact, we have found numerically that the only way in which Eq. (3.15) can be solved is with the trivial solution in which $A_0 = A_L$. We conclude that the momentum jump conditions are not valid in general for two-phase flow though, at this point, it is not clear why this is the case. Allied with our comments in Appendix B concerning the advisability of proposing momentum jump conditions for averaged equations, we dispense with Eq. (3.15) altogether, and the remaining equations will therefore provide a one-parameter family of traveling wave solutions, just as was found in Ref. 31.

Finally, we note that the prescription (B7) of the bubble volume flux q in Appendix B yields

$$\int_{A_0}^{A_L} \frac{(K + cA)J(A)dA}{B(A)} = qL.$$

(3.18)

2. Numerical shock solutions

The mathematical problem for the shock solutions thus reduces to the determination of six constants: L is the wavelength or period of the wave, c is the shock speed, K is an auxiliary integration constant, A_0 and A_L are the values of the liquid fraction at each end of the wave ($z=0, z=L$), and an extra auxiliary constant $\bar{A}$ which is a particular value of the liquid fraction (between A_0 and A_L) defined by Eq. (3.17). The system of equations (3.14), (3.16), and (3.18) provides between them *five equations for the six unknowns* (we seek a one parameter family of solutions).

Our strategy to solve these equations is the following. Suppose we know $\bar{A}$. Then from Eq. (3.17), K is a linear function of c and since J is quadratic in K and c, we can use Eq. (3.17) to find c and K as functions of $\bar{A}$.

Next, $J(A)$ is a rational function of A so the integral in Eq. (3.16) can be computed explicitly as a function $F(A_L, A_0; \bar{A})$. In a similar way, Eq. (3.18) can be written [using Eq. (3.14)] in the form $G(A_L, A_0; \bar{A}) = q$, on defining the appropriate function G. Note that in Eqs. (3.18) and (3.14) since both J and B vanish at $A = \bar{A}$, it is wise to remove the factor $A - \bar{A}$ from J and B in the integrals. Given $\bar{A}$ and the prescribed value of q, we solve the two algebraic equations $F = G - q = 0$, thus determining A_0 and A_L in terms of $\bar{A}$. In this way, we obtain the one parameter family of travelling waves.

In practice, it is convenient to replace the prescription of q by the prescription of A_L. Then, the solution of $F = 0$ yields $A_0(A_L, \bar{A})$, when L and q can be computed directly.

Figure 4 shows a direct numerical computation of the periodic traveling waves which result from solving Eq. (2.22) with $\varepsilon=0.05$ and $\eta^*=1$. These waves arise through an
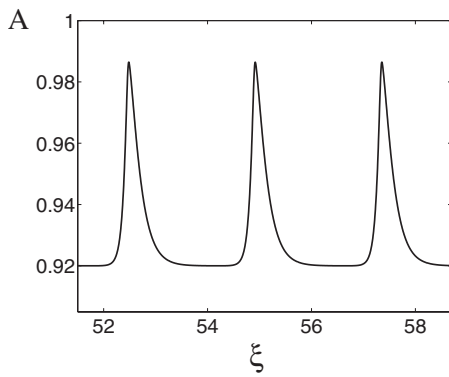
FIG. 4. Periodic waves produced in a direct numerical computation of Eq. (2.22) using values $\varepsilon=0.05$, $\eta^*=1$, which arise from the instability of a uniform state with $A=A^*=0.92$ and $w^*=0.0245$.

FIG. 6. $\bar{A}_\infty$ determined as a function of A_L. $\bar{A}_\infty$ is the limiting value of $\bar{A}$ as $L \rightarrow \infty$, as given in Eq. (3.14), computed by using the shock solutions of the reduced hyperbolic model with $\varepsilon=0$.

instability of a uniform state $A=A^*$, taken here to be $A^*=0.92$. The waves travel backward at a speed $c=-0.26$.

The results of numerical computations such as in Fig. 4 can be compared to the theoretical predictions from the traveling wave analysis. A difficulty in this exercise is that the traveling wave analysis only yields a one parameter family of solutions and it is unclear *a priori* which member of this family should be used. The waves which arise from a uniform state $A=A^*$ typically have $A_L \approx A^*$ so that this provides the appropriate value of A_L. It is also found that the computed waves are long waves, as indicated in Fig. 5. This figure plots the variation of the predicted wavelength L as a function of $\bar{A}$, for three different values of A_L. Also shown are the values of the wavelength of the waves which result from direct computation at the corresponding values of $A^*=A_L$. It can be seen that as $\bar{A}$ increases, L increases without bound as $\bar{A}$ approaches an asymptotic value, which we denote as $\bar{A}_\infty$. This asymptote occurs because the function $B(A)$ has a second zero at a value larger than $\bar{A}$, and the asymptotic value $\bar{A}_\infty$ occurs when this zero merges with $\bar{A}$.

The advantage of the existence of this asymptote is that, providing we assume that long waves are preferentially selected, we can use L as the parameter describing the waves,

but the consequent value of $\bar{A}$ is then given by $\bar{A}_\infty$, and is determined directly by A_L, as illustrated in Fig. 5. In particular, the quantities c and A_0 are then predicted uniquely by A_L and these values can be compared to the results of direct computations. Figure 6 shows the variation of $\bar{A}_\infty$ with A_L determined from the traveling wave analysis. It is a smoothly increasing function, with an apparent limit of $\bar{A}_\infty=1$ at $A_L=1$.

Figures 7 and 8 provide the consequent comparison of the predicted A_0 and c, respectively, with the directly computed values. It can be seen that the agreement is good, well within the $O(\varepsilon)$ error we might expect. The error also appears to dwindle as $\bar{A}_\infty$ (and thus also A_L) approaches one. In addition, the numerical results approach the predictions more and more closely as ε is decreased.

IV. THE NUMERICAL ALGORITHM FOR FINITE ε

Numerical solutions of the full model (2.22) with $\varepsilon \ll 1$ were obtained by using a finite difference method with a uniform grid. We first solved Eq. (2.22a) explicitly for A by using a forward difference for the time derivative and a back-
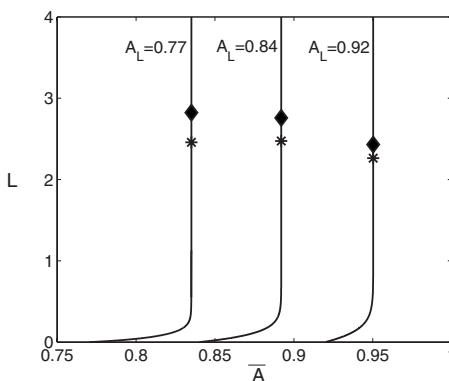

FIG. 5. $L(A_L, \bar{A})$ computed from the reduced hyperbolic model (3.14) for three different values of A_L. The diamonds and stars correspond to values of L obtained numerically from the full equation (2.22) with $\varepsilon=0.05$ and 0.03, respectively, for the same value of A_L, taken to be the uniform state.
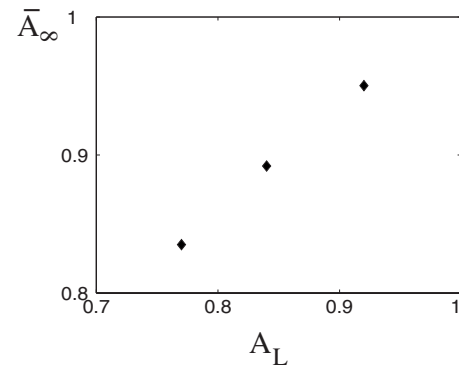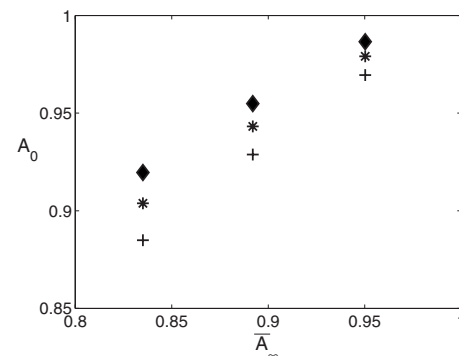

FIG. 7. The diamonds and stars represent values of A_0 obtained via numerical solution of the full model (2.22) (with $\varepsilon=0.05$ and 0.03, respectively, and $\eta^*=1$) at the three values of A_L in Fig. 5, but plotted against the values $\bar{A}_\infty$, which are shown in Fig. 6, and computed from the shock wave analysis of the reduced model with $\varepsilon=0$. The crosses are the values of A_0 predicted directly from the shock wave analysis. Thus, the diamonds and stars represent the "data" or the "exact answer," the crosses are the prediction or the approximate answer.
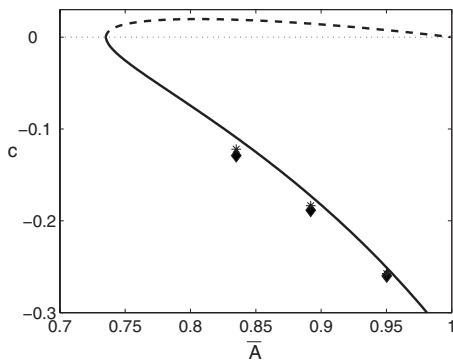
FIG. 8. Computations of the wave-speed c using the full model (2.22) with $\varepsilon \ll 1$. The "exact" values of c (diamonds $\varepsilon=0.05$, stars $\varepsilon=0.03$) are shown as a function of $\bar{A}_\infty$ compared to the solution of the approximate reduced model ($\varepsilon=0$) obtained from solving Eq. (B15) to find $c(\bar{A})$, with $\bar{A}=\bar{A}_\infty$.

FIG. 9. A typical still frame from which flow characteristics are assessed.

ward difference for the spatial derivative. We then solved Eq. (2.22b) implicitly for w. As before, we used a forward difference for the time derivative and since this equation with $\varepsilon \neq 0$ is parabolic, we used central differences for the first spatial derivatives. To obtain an approximation to the second order diffusive term, we used a forward difference for the inner derivative followed by a backward difference for the outer one.

Our approach in modeling the evolution of a small perturbation to the uniform state (A^*, w^*) consisted of applying a small perturbation to the initial condition and allowing it to develop in time. At the inlet boundary both A and w were held constant and $w_\xi=0$ was applied at the outlet. Initial conditions were taken as

$$A(\xi,0) = A^* + \delta(e^{-k_c^2(\xi-\xi_0)^2} - e^{-k_c^2\xi_0^2}), \quad w(\xi,0) = w^*, \qquad (4.1)$$

where k_c is the most unstable wave number and $\delta \ll 1$. Step sizes of $\Delta\xi=5\Delta t=0.005$ and $\Delta\xi=5\Delta t=0.0025$ were used when $\varepsilon=0.05$ and $\varepsilon=0.03$, respectively. The assumption of a zero total volume flux, i.e., $j=0$, results in waves traveling in the negative ξ direction, i.e., upward. However, a value of j sufficiently large in absolute value results in downward traveling waves [see Eq. (2.21)].

We note that the linear theory of Sec. III A was successful in predicting when roll waves would develop in the full nonlinear model (any numerical simulations shown here occurred in the linearly unstable region of parameter space). We also note that the dimensional time for the periodic waves to evolve from the initial condition was typically of the order of one second. In practice, the waves seem to occur almost instantaneously.

V. DISCUSSION

We have examined high speed digital video images of settling Guinness to obtain estimates of such quantities as bubble size and void fraction. Figure 9 shows a typical image of this type. From these images, we are able to calculate bubble size and void fraction, and also wave speed and wavelength. All of these quantities vary somewhat depending on the position in the glass, and also with time since pouring.
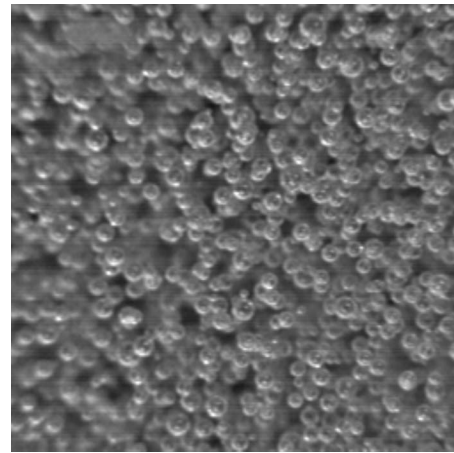
Bubble sizes from one frame are shown in Fig. 10. They are approximately normally distributed, with a mean diameter of 122 μm ($a=61$ μm); another image produced a normal distribution with smaller mean radius, 47 μm. The density of Guinness is determined from its specific gravity, which is the ratio of its density to that of water. The SG is taken as 1.007, from information provided by Roche at Diageo (manufacturers of Guinness). The density of water varies a little with temperature, decreasing from 10^3 kg m^{-3} at 5 °C to 0.9982×10^3 kg m^{-3} at 20 °C so we take $\rho_l \approx 10^3$ kg m^{-3}. The viscosity is not apparently publicly available and we have measured it. We find that at a temperature of about 5 °C, the viscosity is $\mu \approx 2 \times 10^{-3}$ Pa s.

Although the waves are easily seen in video (or in the flesh), they are difficult to isolate on still images. Figure 11 shows one such image where the wave crests are indicated. In this image, the wave spacings are 5.3, 5.9, 6.4, 6.7, 6.7, and 7.0 mm from top to bottom. Identification of wave spacings is also awkward because the waves are themselves sub-
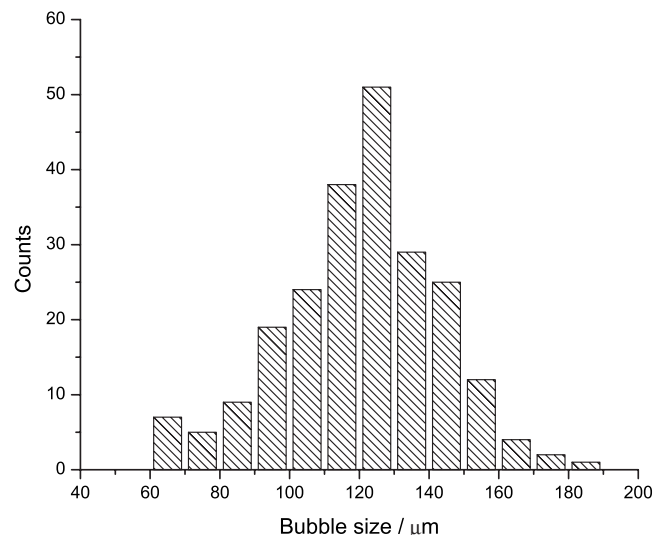

FIG. 10. Histogram of bubble sizes in diameters, from an image about two-thirds up the glass. The mean diameter is 122 μm and there is quite a wide distribution.
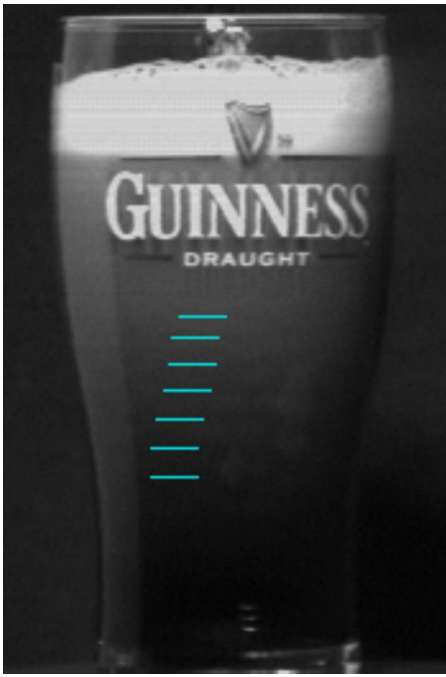
FIG. 11. (Color online) The horizontal dashes mark visually defined wave crests in the Guinness.

ject to a lateral instability which causes them to be corrugated (see Fig. 1).

The wave profiles are quite distinct. The waves consist of 4–5 mm length regions of bubbles, separated by plugs of bubble-free pure fluid, some 1.4–1.8 mm in length. These correspond to parts of the wave where $A=1$, and are not described in the present theory. Figure 12 shows a histogram of measured wave speeds, with mean 20.9 mm s^{-1}. Wave speed was measured in two ways. First, local zoomed video clips were examined and wave speed was measured from the differing plug positions in separate frames. These clips were taken from video shot at 750 frames/s.

A second method was to look at a whole glass shot, measuring distance traveled versus frame number, shot at
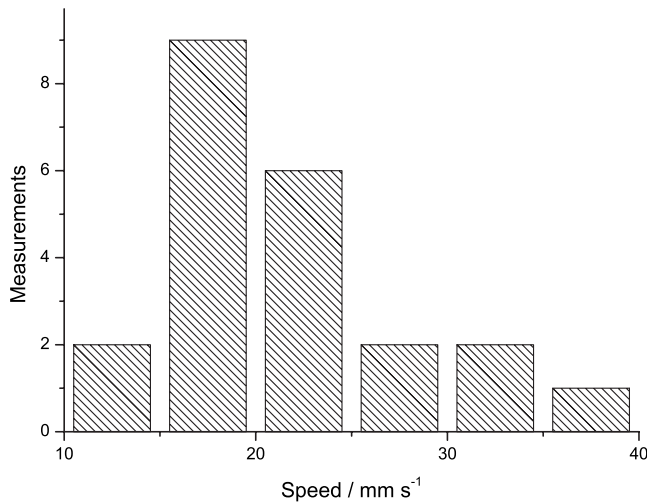

FIG. 12. Histogram of wave speeds. The mean is 20.9 mm s^{-1} and the distribution is skewed toward higher wave speeds.

125 frames/s. This latter method gave a single result of 21.8 mm s^{-1}, which is in good agreement with the zoomed result.

The average void fraction of bubbles was measured from still video frames, such as that shown in Fig. 9. With short depth of focus, one can estimate an areal bubble fraction, and with a measured mean bubble radius, and the assumption of uniform bubble packing, it is straightforward to estimate the bubble volume fraction α. Obviously, this changes with location and time, tending to zero at late times and deep position. From four different images, low on the glass and early in the settling, we measured $\alpha=0.237$, 0.233, 0.242, and 0.266. At a higher location, about a centimeter below the accumulating head, we found $\alpha=0.315$.

The form of the waves computed in Fig. 4 can be compared to some extent with these observations. The computed wave consists of two parts, a flat region at low A (high α) and a thin spike where A is large. The relative lengths of the two regions are the same as in the observations (about a third), except that in the experiment, the values are more extreme: $A=1$ in the spike (bubble-free liquid) and $A \approx 0.75$ in between. Our model is not able to approach or attain such high amplitude waves, at least with the parametric choices we have made, but it is qualitatively similar.

To compute the length and velocity scales, we use median bubble radius $a=6.1 \times 10^{-5}$ m, density $\rho_l=10^3$ kg m^{-3}, viscosity $\mu_l=2 \times 10^{-3}$ Pa s, and acceleration due to gravity $g=9.81$ m s^{-2}. From Eq. (2.7), we then compute

$$l = 0.034 \text{ mm}, \quad u_0 = 18.25 \text{ mm s}^{-1}. \tag{5.1}$$

These values need to be compared to observed wavelengths and wave speeds.

The observed wavelength is $L_D \approx 6$ mm and this corresponds to a dimensionless wavelength

$$L = \frac{L_D}{u_0} \approx 180. \tag{5.2}$$

This is much larger than the numerically computed values $L \approx 2.4$–2.8, although the result is consistent with a tendency toward long wavelength selection. We have no explanation for why such long wavelengths might be selected, but we merely note that the observations are not inconsistent with the theory.

The theory does much better with the wave speed, which, as we have said, provides a genuine test of the traveling wave theory, given long waves. If the background dimensional flux defined [compare Eq. (2.11)] by

$$j_D = \alpha v_D + (1 - \alpha)u_D \tag{5.3}$$

is negative (i.e., the mixture is going downward, as we infer), then the dimensional wave speed downward will be

$$c_D = u_0 c_0 + |j_D|, \tag{5.4}$$

where c_0 is the theoretical wave speed at zero net flux, shown in Fig. 8. It is difficult to estimate j_D since we cannot estimate liquid velocity. If it is comparable to the velocity mechanically induced by pouring, then, we expect $|j_D| \sim 10$–25 mm s^{-1}, while for values of $c_0 \approx -0.2$ (see Fig. 8) and with $u_0=18$ mm s^{-1}, observed wave speeds of

21 mm s^{-1} are obtained for $|j_D| \approx 24.6$ mm s^{-1}. This result is encouraging. As the pint settles, we might then expect $|j_D|$ to decrease, causing the waves to slow down, as observed.

VI. CONCLUSIONS

We have presented a two-phase flow theory for bubbly flow, with the intention of explaining why waves form in such flows, and in particular why they form in poured pints of Guinness, and also why they go downward. The theory is able to explain wave formation via instability of a uniform flow and the results seem reasonably consistent with observations. In particular, the wave speed is well explained. The wavelength of the observed waves is much longer than one would predict but this observation of itself does not invalidate the theory. It merely raises the question of how the wavelength of the waves is selected since the theory is only able to provide a one parameter family of traveling wave solutions (with the wavelength being the parameter of the family). In fact, a similar conundrum besets the phenomenon of roll waves in inclined channel flows, and it is a matter of common observation that the waves observed on an inclined pavement during heavy rain, for example, have wavelengths much longer than their depth. This suggests that the issue of wavelength selection is not an immediate fault of the present model.

The model is, however, not at all perfect. While the choice of the added virtual mass and interfacial pressure terms seems reasonable, there are other possibilities, and the choice of the coefficients C_{VM} and H is at least uncertain. A particularly desirable improvement would be to have a model which produced waves in which slugs of high void fraction ($\alpha \approx 0.25$) alternated with plugs of pure liquid. The high void fraction is near the value where the bubbly two-phase flow equations are expected to break down, and this suggests that the waves of clear liquid are a manifestation of regime transition. We have not been able to find similar behavior, although in truth it would be difficult to compute even if it were there.

Are there any other mechanisms which might produce the waves? One possibility is a hindering effect due to the bubble size distribution. Large bubbles tend to rise more rapidly than small bubbles, and so in a distribution one can expect a separation effect, and the formation of waves similar to those which occur in the traffic along a two lane road, and familiar to all commuters on such roads, where rapidly moving cars accumulate in queues behind isolated, more slowly moving trucks. Whether such a mechanism is viable in three-dimensional flow is unclear (it is fairly infrequent even on three lane motorways) and it is even less clear how one might model the process. Another possibility is that the waves are a manifestation of a Tollmien–Schlichting instability in the shear flow of the liquid in the glass. An assessment of this possibility may be made through an estimate of the Reynolds number of the flow. With a velocity of 0.02 m s^{-1} and a glass radius of 0.04 m, we find a Reynolds number of about 800. This is well below the value at which transition to turbulence sets in for a pipe flow and, in addition, we note that such transitions are generally seen in forced, not naturally convective, flows. Furthermore, regular waves are only seen if they are excited, for example, by a vibrating ribbon. We consider such an instability an unlikely cause for the waves.

APPENDIX A: DERIVATION OF THE MODEL

In this appendix, we justify the basic model (2.1), discuss the boundary conditions appropriate for the problem, and introduce a regularizing bulk or eddy viscosity. The most basic set of equations describing one-dimensional adiabatic two-phase flow in a pipe is the following:

$$\alpha_t + (\alpha v)_x = 0, \tag{A1a}$$

$$-\alpha_t + [(1-\alpha)u]_x = 0, \tag{A1b}$$

$$\rho_l(1-\alpha)(u_t + uu_x) = -(1-\alpha)\frac{\partial p_l}{\partial x} + F_{gi} - F_{lw}, \tag{A1c}$$

$$\rho_g \alpha(v_t + vv_x) = -\alpha\frac{\partial p_g}{\partial x} - F_{gi}. \tag{A1d}$$

The variables are the void fraction α, the averaged gas and liquid velocities v and u, and the gas and liquid pressures p_g and p_l; x denotes the long axis distance, and F_{gi} and F_{lw} are the frictional resistance exerted on the gas by the liquid (at the gas-liquid interface) and the wall friction exerted on the liquid (it is assumed that the flow is fully turbulent), respectively. It is usual to constitute these two terms algebraically in terms of u and v and they represent the integrated effects of the Reynolds (shear) stresses in each phase.

The derivation of phase-averaged equations has been discussed by many authors, for example, Refs. 19–21 and 35. A constitutive relation between p_g and p_l is necessary in Eq. (A1) and we simply assume that

$$p_g = p_l = p. \tag{A2}$$

While the model (A1) makes several unwarranted assumptions (for example, that the average $\langle u^2 \rangle$ is equal to the square of the average, $\langle u \rangle^2$), it appears at first sight to be physically plausible. It is thus disconcerting to find that its characteristic speeds $dx/dt = \lambda$ are given by ∞, ∞ (corresponding to two infinite sound speeds, as we assume ρ_l and ρ_g are constant), and the two values

$$\lambda = \frac{u \pm isv}{1 \pm is}, \tag{A3}$$

where

$$s = \left[\frac{\rho_g(1-\alpha)}{\rho_l \alpha} \right]^{1/2}. \tag{A4}$$

If $u \neq v$, the characteristics are complex and the model is ill posed, requiring that the data be prescribed in the future. High wave number perturbations to a uniform state are of the form $e^{ik(x-\lambda t)}$, with growth rate $k \, \text{Im} \, \lambda$ which is unbounded as $k \to \infty$.

This indicates that there is something *fundamentally* wrong with the simple model (A1). Computationally, it is apparently sometimes less so since often $\rho_g \ll \rho_l$, so that the characteristics are only "mildly" complex $[\text{Im} \, \lambda = O(s) \ll 1]$, and this, together with the suppression of high wave numbers on a finite grid and numerical diffusion, may remove the problem in practice.

It is also easy to fix. For example, the effect of averaging nonlinear terms is often represented by the use of a profile coefficient. Specifically, the acceleration of the liquid might be written as $u_t + D_l u u_x$, where the choice of $D_l \neq 1$ represents the effect of a nonuniform cross sectional profile. An example is in annular flow, where the film flow has a profile coefficient (when laminar) of $D_l = 4/3$. On the other hand, the two (finite) characteristics are given, see Ref. 28, as the solutions of

$$(\lambda - u)^2 = -s^2(\lambda - v)^2 + (D_l - 1)[u^2 + 2u(\lambda - u)], \tag{A5}$$

and when s is small, these are both real if

$$D_l \gtrsim 1 + [s(u-v)/u]^2, \tag{A6}$$

which is easily satisfied if $\rho_g \ll \rho_l$.

There are other possibilities: a more general derivation of the momentum equation of (for example) the liquid leads to (here, assuming the profile coefficient $D_l = 1$)

$$\rho_l(1-\alpha)[u_t + u u_x] = -(1-\alpha)\frac{\partial p_l}{\partial x} + \Delta p_{li}\frac{\partial(1-\alpha)}{\partial x}$$
$$+ C_{\text{VM}}\alpha\rho_l[(v_t + v v_x) - (u_t + u u_x)]$$
$$+ F_{gi} - F_{lw}, \tag{A7}$$

where C_{VM} is the virtual mass coefficient, of order one, and $\Delta p_{li} = p_{li} - p_l$ represents the average difference between the liquid interfacial pressure and the liquid pressure. It is possible to include other terms in this equation as well. A suitable choice of the interfacial pressure change is

$$\Delta p_{li} = -H\rho_l(v-u)^2, \tag{A8}$$

where $H = \frac{1}{4}$ (see Ref. 36), and both this and the use of a nonzero virtual mass coefficient can easily lead to real-valued characteristics. Recent work in this direction is that of Refs. 37 and 38. Although it is thus easy to rescue the hyperbolicity of the model, the unease due to the demonstration of ill-posedness of Ref. 15 remains (as discussed in Sec. I). The view we take is that the instability of the model always precedes the onset of ill posedness (resulting from the presence of complex characteristics), which we suppose leads to a regime transition. In this paper, we suggest that this is the case for bubbly two-phase flow.

For the remainder of this section, we consider for algebraic simplicity the regularizing effects of a liquid profile

coefficient $D_l \neq 1$. Our final model will be in a form more suitable for the description of bubbly flow, including virtual mass effects. However, the general points we make below do not rely on the details of how the model is regularized.

1. Boundary conditions

It is convenient to think in terms of the basic model (A1), if some adjustments (such as $D_l > 1$ or $C_{\text{VM}} > 0$) are made to ensure hyperbolicity. Experiments such as those to determine regime diagrams are done in very long pipes (>10 m length). The diagrams are determined in terms of two parameters, which can be taken to be the liquid and gas mass fluxes, G_l and G_g, and these are determined by the experimentalist: (s)he can control two inlet taps. In addition, it is reasonable to assume that the outlet pressures of each phase are equal to each other and to a prescribed exit pressure of the outlet tank. Apparently, these are the only physically appropriate conditions to prescribe.

However, this is not a sufficient number of conditions for the basic two-phase flow model (A1) or any of its hyperbolic variants. Suppose that $p_l = p_g = p$ but (say) $D_l > 1$ so that Eq. (A1) is hyperbolic. Total mass conservation yields

$$\alpha v + (1-\alpha)u = \frac{G_l}{\rho_l} + \frac{G_g}{\rho_g}, \tag{A9}$$

thus, $v = v(\alpha, u)$, while elimination of $\partial p / \partial x$ gives

$$\rho_l(u_t + D_l u u_x) - \rho_g(v_t + v v_x) = \frac{F_{gi}}{\alpha(1-\alpha)} - \frac{F_{lw}}{1-\alpha}, \tag{A10}$$

and together with Eq. (A1b), we have a pair of hyperbolic equations for α and u, with one boundary condition, that $\alpha u = G_l / \rho_l$ on $x = 0$. The prescribed outlet pressure then determines p if α, u (and thus, v) are known. However, the solution of Eqs. (A10) and (A1b) also requires α to be prescribed at $x = 0$.

2. Entry length

If α, G_l, and G_g are all prescribed at the inlet, this appears to suggest that regime diagrams should also depend on $\alpha_0 = \alpha|_{x=0}$; but experimentally, this appears not to be the case. To understand this, suppose that the acceleration terms in Eq. (A1) are negligible. Then,

$$-\frac{\partial p}{\partial x} = \frac{F_{gi}}{\alpha} = \frac{F_{lw} - F_{gi}}{1-\alpha}, \tag{A11}$$

thus

$$F_{gi} = \alpha F_{lw}, \tag{A12}$$

and this defines an algebraic relation between α, u, and v. One usually defines

$$F_{lw} = \frac{4}{d} f_w \rho_l |u|u, \quad F_{gi} = \frac{4}{d} f_i \rho_g |v - \chi u|(v - \chi u), \tag{A13}$$

where d is the pipe diameter and χ is a factor which takes account of the regime: $\chi = 2$ is appropriate in annular flow, for example. The friction factors f_w and f_i depend on α and

also on u (respectively, v) via the Reynolds number of each phase. Mass conservation of each phase yields

$$(1 - \alpha)u = G_l/\rho_l, \quad \alpha v = G_g/\rho_g, \tag{A14}$$

so that Eqs. (A12) and (A14) determine α, u, and v; evidently, the value of α is not necessarily that at the inlet.

In a tube of length l, the liquid and gas acceleration are of order $\rho_l u^2/l$ and $\rho_g v^2/l$, respectively, whereas the wall friction is given in Eq. (A13). The ratio of the acceleration to the friction terms is thus (for the liquid),

$$\delta_w = \frac{(\rho_l u^2/l)}{(4f_w \rho_l u^2/d)} = \frac{d}{4f_w l}, \tag{A15}$$

and the equivalent ratio for the gas terms is

$$\delta_i = \frac{(\rho_g v^2/l)}{(4f_i \rho_g v^2/d)} = \frac{d}{4f_i l}. \tag{A16}$$

The typical pipe dimensions might be $d=2$ cm, $l=10$ m, while a typical value of f_i and f_w is 0.005.[39] In this case, $\delta_{i,w} \sim 0.1$ and for longer pipes, these parameters are smaller. The relatively small values of $\delta_{i,w}$ indicate that in such long pipes, the acceleration terms can indeed be neglected, and this confirms that the flow regime can be expected to depend only on the inlet mass fluxes.

3. Bulk and eddy viscosity

The basic simple model (A1) has complex characteristics if $u \neq v$ (but even if $u=v$, the characteristics are repeated, and the system is still ill-posed). We must, thus, choose to rescue the reality of the characteristics by such (realistic) quantities as profile coefficients, interphase pressure jumps, and virtual mass coefficients. However, these simply postpone the ill-posedness of the system; for example, Ref. 14 postpones the complexity of the characteristics until a critical value of α of about 0.25 (in bubbly flow).

Despite the specter of ill posedness, it has often been suggested that complexity of characteristics is a manifestation of a physical instability, as in the transition from bubbly to slug flow.[14] In Sec. III, it was demonstrated that the nonlinear evolution of such instabilities leads to shock formation of the underlying hyperbolic system. Such shocks must be smoothed by higher order diffusive terms and we now discuss the origin of these.

We expect that three-dimensional two-phase equations involving some kind of (eddy) viscosity would be well posed, and the problem in the one-dimensional models arises in some way through the replacement of the second derivative viscous terms by algebraic friction terms. These terms are based coherently on the successful use of Prandtl's mixing length theory and seem to be entirely reasonable. However, if we are willing to adopt an eddy viscosity model for the shear stress, then, we must logically allow for normal stresses to be similarly constituted. This then suggests the inclusion of an eddy viscous term in the liquid momentum equation, as was included by Refs. 20 and 29. The form we suppose for such a term on the right hand side of Eq. (A1c) is

$$\frac{\partial \tau_l}{\partial x}, \quad \tau_l = \eta(1 - \alpha)\frac{\partial u}{\partial x}, \tag{A17}$$

where η is an appropriate eddy viscosity.

For a more or less laminar flow, we might expect such eddy effects to be small but another term of similar type arises as a "bulk" viscosity (see Ref. 40), which occurs because of the time dependent contraction of bubbles. The average induced strain rate of the bubbles is proportional to the difference between average liquid pressure p_l and average interfacial pressure, which we take to be the gas pressure, thus

$$p_g - p_l = \eta\left(\frac{\partial \alpha}{\partial t} + u_i\frac{\partial \alpha}{\partial x}\right), \tag{A18}$$

where for a dilute collection of bubbles,

$$\eta = \frac{4\mu}{3\alpha}, \tag{A19}$$

with μ being the liquid viscosity; u_i is the average interfacial velocity, which we take to be v (because that is the actual average interfacial velocity). By using the conservation of mass equations, we find that Eq. (A18) can be written in the form

$$p_g - p_l = \eta(1 - \alpha)u_x, \tag{A20}$$

if we neglect gradients in α. The consequence of a term like this in addition to the average interphasic pressure difference term is also to introduce an effectively viscous term into the equations.

Thus, both the existence of continuous phase fluid turbulence and also the dynamical interfacial effects of interphasic pressure differences in a bubbly flow will lead to an effective bulk or eddy viscous term, whose magnitude can be substantially larger than that due to molecular viscosity. It can also be mentioned that the Faxen force contributes a similar term. We use a regularizing term of this type when solving the model numerically.

4. Stability and ill-posedness

We consider the inclusion of the bulk or eddy viscosity term in the basic model (A1) (still with $p_g=p$ but including a profile coefficient for the liquid)

$$\alpha_t + (\alpha v)_x = 0, \tag{A21a}$$

$$-\alpha_t + [(1 - \alpha)u]_x = 0, \tag{A21b}$$

$$\rho_g(v_t + vv_x) = -\frac{\partial p}{\partial x} - \frac{F_{gi}}{\alpha}, \tag{A21c}$$

$$\rho_l(u_t + D_l uu_x) = -\frac{\partial p}{\partial x} + \frac{1}{1 - \alpha}\frac{\partial}{\partial x}\left[\eta(1 - \alpha)\frac{\partial u}{\partial x}\right]$$
$$+ \frac{F_{gi} - F_{lw}}{1 - \alpha}, \tag{A21d}$$

and elimination of p yields

$$\rho_l(u_t + D_l u u_x) - \rho_g(v_t + v v_x)$$

$$= \frac{1}{1-\alpha}[\eta(1-\alpha)u_x]_x + \frac{F_{gi}}{\alpha(1-\alpha)} - \frac{F_{lw}}{1-\alpha}. \qquad (A22)$$

As before, conservation of mass gives $v=v(\alpha,u)$ so that α and u are governed by Eqs. (A21b) and (A22), and we prescribe both α and u at the inlet. The prescription of $p_g=p_l=p_{ex}$ at the outlet determines p there, and also forces $u_x=0$, if we assume Eq. (A20). Thus, the apparently diffusive equation for u has naturally prescribed boundary values at inlet and outlet, while the hyperbolic equation for α has an initial condition. This model is well-posed (in a sense we will explain). However, the ill-posedness of the diffusionless model is manifested through an instability.

To see this, let us examine the approximation where the gas acceleration terms are neglected, and we write [cf. Eq. (A10)]

$$-\alpha_t + [(1-\alpha)u]_x = 0,$$

$$u_t + D_l u u_x = \nu u_{xx} + R(\alpha,u), \qquad (A23)$$

where

$$R(\alpha,u) = \frac{1}{\rho_l}\left[\frac{F_{gi}}{\alpha(1-\alpha)} - \frac{F_{lw}}{1-\alpha}\right], \qquad (A24)$$

$D_l \geq 1$, we suppose $\nu = \eta/\rho_l$ is constant, and have for simplicity ignored the terms in α in the bulk viscous term. If α^*, u^* is a steady solution, then small perturbations proportional to $\exp(ikx+\sigma t)$ satisfy Eq. (A23) provided $\hat\sigma = \sigma + iku^*$ satisfies

$$\hat\sigma^2 + (ikdu^* + \nu k^2 + |R_u|)\hat\sigma - ik(1-\alpha^*)R_\alpha = 0, \qquad (A25)$$

i.e.,

$$\sigma = -iku^*\left(1 + \frac{1}{2}d\right) - \frac{1}{2}(\nu k^2 + |R_u|)$$

$$\times\left\{1 \pm \left[\left(1 + \frac{ikdu^*}{|R_u| + \nu k^2}\right)^2 + \frac{4ik(1-\alpha^*)R_\alpha}{(|R_u| + \nu k^2)^2}\right]^{1/2}\right\}, \qquad (A26)$$

where we write $d=D_l-1$ and assume realistically that $R_u < 0$. If we define the square root in Eq. (A26) as $p+iq$, $p > 0$, then

$$p^2 - q^2 = 1 - \left(\frac{kdu^*}{|R_u| + \nu k^2}\right)^2,$$

$$pq = \frac{kdu^*}{|R_u| + \nu k^2} + \frac{2k(1-\alpha^*)R_\alpha}{(|R_u| + \nu k^2)^2}. \qquad (A27)$$

Writing

$$M = \frac{kdu^*}{|R_u| + \nu k^2}, \quad N = \frac{2k(1-\alpha^*)R_\alpha}{(|R_u| + \nu k^2)^2}, \qquad (A28)$$

we have $pq=M+N$, $p^2-(M+N)^2/p^2=1-M^2$, and since the criterion for instability is that $p > 1$, we see that instability

occurs if and only if $1-M^2 > 1-(M+N)^2$, i.e., (assuming $R_\alpha < 0$)

$$\frac{(1-\alpha^*)|R_\alpha|}{|R_u| + \nu k^2} > du^*. \qquad (A29)$$

The relationship between instability and characteristics is this. The characteristics $dx/dt=\lambda$ (of the equations when $\nu=0$) are given by the values $-\sigma/ik$ in the high wave number limit $k\to\infty$, or equivalently if $R\equiv 0$. If we examine Eq. (A29), we see that the basic state is always unstable (for $R \neq 0$) if $d=0$, i.e., $D_l=1$. However, we know that the model is ill-posed if $d=0$ and $\nu=0$. If $\nu\neq 0$, the basic state may still be unstable, but if we write

$$a = \nu + \frac{idu^*}{k} + \frac{|R_u|}{k^2}, \quad b = (1-\alpha^*)|R_\alpha|, \qquad (A30)$$

then we have, as $k\to\infty$,

$$\hat\sigma \approx -\frac{ib}{ka} + \frac{b^2}{k^4 a^3} + \dots, \qquad (A31)$$

and expanding a^{-1} for large k, we find

$$\text{Re}\,\hat\sigma \approx -\frac{bdu^*}{\nu^2 k^2}\left(+\frac{b^2}{\nu^3 k^4}\dots\right), \qquad (A32)$$

where the second term is the leading term if $d=0$. Thus, even though all modes are unstable if $d=0$, their growth rate tends to zero; and if $d > 0$, high wave number modes are damped.

Hence, we suggest that while eddy (or bulk) viscosity regularizes the model in the sense that high wave number growth rates become very small, it is still necessary to include terms such as the profile coefficients, or the virtual mass terms, in order to damp these high frequency modes. We also see that as D_l is reduced toward unity, instability always occurs before the ill-posed limit is reached.

APPENDIX B: SHOCK CONDITIONS

In this appendix, we discuss jump conditions across the shock and the analysis of the shock structure.

1. Momentum jump condition

Across the shock at $z=0$ (or $z=L$), we would naturally propose jump conditions associated with the conservation of mass and momentum. There are two mass conservation equations but only one mass jump condition (say for the liquid), because the total flux integral (2.11) then automatically ensures that mass of gas is conserved. If a shock is located at the dimensional position $x=x_s$, then the mass jump condition can be written in the (dimensional) form

$$\dot{x}_s = \frac{[(1-\alpha)u]_-^+}{[1-\alpha]_-^+}. \qquad (B1)$$

We can also write a jump condition representing the conservation of total momentum. We add the two momentum equations in Eq. (2.1) (ignoring the bulk diffusive term) and apply the usual box integral condition to obtain the jump condition

$$\dot{x}_s = \frac{[\rho_l(1-\alpha)u^2 + \rho_g\alpha v^2 + (1-\alpha)p_l + \alpha p_g]_-^+}{[\rho_l(1-\alpha)u + \rho_g\alpha v]_-^+}. \quad (B2)$$

It is important to realize that a single jump condition for momentum is the maximum we can hope to obtain. Momentum of each phase is not conserved across a shock, most simply because the derivative terms in the virtual mass coefficients allow momentum jumps, although these terms represent interfacial forces at the microscopic scale. In particular, the pseudomomentum equation (2.22b) appears not to be a conservation law, and it is inadmissible to try to derive a jump condition from it. This explicitly contradicts the discussion in Ref. 20 (p. 288). However, although the pseudomomentum equation does not support a conservation jump condition, it does support a shock structure (for $\varepsilon \ll 1$), and this leads to a *different* jump type condition which must be satisfied.

Consider a conservation law of the form

$$\rho_t + q_x = \varepsilon[J(\rho, \rho_x)]_x, \quad (B3)$$

where $\partial J/\partial \rho_x > 0$, $J(\rho, 0)=0$, and $q=q(\rho)$. When $\varepsilon = 0$, shocks may form whose speed is given by

$$c = \frac{(q)_-^+}{(\rho)_-^+}, \quad (B4)$$

and this result may be derived *either* by first principles integral conservation of ρ *or* by analyzing the shock structure when $\varepsilon \ll 1$.

We may take the view that the shock structure derivation is the more fundamental and certainly, it must be appropriate in describing the solutions of the actual partial differential equations. For the moment, we consider both possibilities but note that while the momentum jump condition (B2) seems reasonable, the whole issue of deriving jump conditions in averaged equations, where local interfacial jumps are constituted, is very problematical. Averaged equations may formally be derived by a multiple scale technique associated with homogenization, in which the small parameter (say, ε_m) is associated with the granularity of the medium, while the shock conditions arise from the diffusion parameter (here, ε) approaching zero. Issues of ordering of the double asymptotic limit $\varepsilon_m \to 0$, $\varepsilon \to 0$ are complex and as yet unresolved.

In dimensionless terms, the shock conditions can be written in the form

$$\dot{x}_s = \frac{[(1-\alpha)u]_-^+}{[1-\alpha]_-^+} = \frac{[(1-\alpha)u^2 + \delta\alpha v^2 + (1-\alpha)p_l + \alpha p_g]_-^+}{[(1-\alpha)u + \delta\alpha v]_-^+}. \quad (B5)$$

An apparently suitable jump condition at $z=L$ follows from Eq. (B5), the second of which after some algebra can be written in the form (note that $\dot{x}_s=-c$)

$$c = \frac{\left(w^2\left\{A\left[1+\frac{H}{(1-A)^2}\right] - \frac{1}{2}C_{VM}\left[\frac{A^2}{(1-A)^2}-1\right]\right\}\right)_{A_0}^{A_L} + \int_{A_0}^{A_L}\frac{AwJ(A)dA}{W(A)B(A)}}{\left[w\left(\frac{C_{VM}}{1-A}+A\right)\right]_{A_0}^{A_L}}, \quad (B6)$$

where $w=(K+cA)/A$. [The first jump condition $c=(Aw)_0^L/(A)_0^L$ is automatically satisfied by Eq. (3.11)]. We note that when written in this form, Eq. (B6) involves the interfacial force coefficients. This inevitably raises doubts concerning the appropriateness of this jump condition.

In addition, we must prescribe the total bubble volume flux. In Guinness, this is not well defined since it depends on the circulatory flow in the glass, but if we imagine flow in a pipe where the inlet volume fluxes of both phases are prescribed as well as the volume fraction, then the average bubble volume flux in the waves must equal that at the inlet. If this is (dimensionally) $u_0 q$ (thus dimensionlessly q), then [using Eq. (3.12)] we have

$$\int_{A_0}^{A_L}\frac{(K+cA)J(A)dA}{B(A)} = qL. \quad (B7)$$

As a practical alternative, we shall find that it may be appropriate to prescribe A_L instead.

2. Shock structure

Equations (3.14), (B6), and (B7) appear to provide three relations for the five unknowns L, c, K, A_0, and A_L. Two further relations follow from an analysis of the shock structure. Having introduced the ε term in Eq. (2.22) to regularize the model, and then subsequently neglected it on the basis that it is small, we now finally see the necessity for such a term. The formation of a shock is physically justified provided a shock structure exists in the limit that ε tends to zero. Near a shock position $\xi=ct$, we set

$$\xi = ct + \varepsilon\zeta \quad (B8)$$

in Eq. (2.22), and at leading order with $\eta^*=1$, we find that A satisfies

$$J(A)A' = -KA^2\left(\frac{A'}{A}\right)', \quad (B9)$$

with

$$A \to A_0 \text{ as } \zeta \to \infty, \quad A \to A_L \text{ as } \zeta \to -\infty. \tag{B10}$$

If

$$I(A) = \int_{A_L}^{A} \frac{J(A)dA}{A^2}, \tag{B11}$$

then the first integral of Eq. (B9) is

$$I(A) = -\frac{KA'}{A}, \tag{B12}$$

with solution

$$\zeta = K \int_A^{\bar{A}} \frac{dA}{AI(A)}, \tag{B13}$$

where $\bar{A}$ is an arbitrary value between A_0 and A_L (we prescribe it precisely below). In order that this describes a satisfactory shock structure, we require $I(A_L) = I(A_0) = 0$, and the second of these implies

$$\int_{A_0}^{A_L} \frac{J(A)}{A^2} dA = 0, \tag{B14}$$

and $I \neq 0$ for A between A_0 and A_L. This provides a fourth relationship among the unknowns.

The satisfaction of Eq. (B14) requires that there should be a value (which we can now define to be $\bar{A}$) such that $J(\bar{A}) = 0$; and then consideration of Eq. (3.12) requires that

$$\bar{A}[W(\bar{A}) - c] = K, \quad J(\bar{A}) = 0, \tag{B15}$$

and this provides the final relationship we require.

In order that ζ increases between A_L and A_0, consideration of Eqs. (3.12), (B11), and (B12) suggests that in order to have a rising wave and descending shock, i.e., $A_0 < A_L$, then $KJ(A_L) < 0$ and $J(A_L)B(A_L) > 0$. Equivalently, for a descending wave and ascending shock with $A_0 > A_L$, then $KJ(A_L) < 0$ and $J(A_L)B(A_L) < 0$. Only solutions satisfying these constraints are admissible as possible voidage wave solutions. These conditions can be concatenated into the pair of relations

$$KJ(A_L) < 0, \quad J(A_L)B(A_L)(A_0 - A_L) < 0. \tag{B16}$$

[1] H. K. Kytömaa and C. E. Brennen, "Small amplitude kinematic wave propagation in two-component media," Int. J. Multiphase Flow **17**, 13 (1991).
[2] A. Matuszkiewicz, J. C. Flamand, and J. A. Bouré, "The bubble-slug flow pattern transition and instabilities of void-fraction waves," Int. J. Multiphase Flow **13**, 199 (1987).
[3] H. Cheng, J. H. Hills, and B. Azzopardi, "A study of the bubble-to-slug transition in vertical gas-liquid flow in columns of different diameter," Int. J. Multiphase Flow **24**, 431 (1998).
[4] G. J. Kynch, "A theory of sedimentation," Trans. Faraday Soc. **48**, 166 (1952).
[5] M. J. Lighthill and G. B. Whitham, "On kinematic waves: I. Flood movement in long rivers," Proc. R. Soc. London, Ser. A **229**, 281 (1955).
[6] M. J. Lighthill, and G. B. Whitham, "On kinematic waves: II, Theory of traffic flow on long crowded roads," Proc. R. Soc. London, Ser. A **229**, 317 (1955).
[7] A. Kluwick, "Roll-waves of low amplitude," Z. Angew. Math. Mech. **58**, 283 (1978).
[8] A. Kluwick, "Wave hierarchies in suspensions of particles in fluids," Z. Angew. Math. Mech. **63**, 264 (1983).
[9] A. Kluwick, "Small-amplitude finite-rate waves in suspensions of particles in fluids," Z. Angew. Math. Mech. **63**, 161 (1983).
[10] A. Kluwick, "The propagation of long waves of small amplitude in suspensions of particles in fluids," Z. Angew. Math. Mech. **65**, 206 (1985).
[11] M. M. El-Kaissy and G. M. Homsy, "Instability waves and the origin of bubbles in fluidized beds, Part I: Experiments," Int. J. Multiphase Flow **2**, 379 (1976).
[12] J. D. Ramshaw and J. A. Trapp, "Characteristics, stability, and short-wavelength phenomena in two-phase flow equation systems," Nucl. Sci. Eng. **66**, 93 (1978).
[13] H. B. Stewart, "Stability of two-phase flow calculation using two-fluid models," J. Comput. Phys. **33**, 259 (1979).
[14] C. Pauchon and S. Banerjee, "Interphase momentum interaction effects in the averaged multifield model, Part I: Void propagation in bubbly flows," Int. J. Multiphase Flow **12**, 559 (1986).
[15] A. Prosperetti and J. V. Satrape, "Stability of two-phase flow models," in *Two-phase Flow Models and Waves*, edited by D. D. Joseph and D. G. Schaeffer (Springer, New York, 1990), pp. 98–117.
[16] A. V. Jones and A. Prosperetti, "On the suitability of first-order differential models for two-phase flow prediction," Int. J. Multiphase Flow **11**, 133 (1985).
[17] S. Patterson, "Peregrinations: Fizz-ics," Photonics Spectra **38**, 194 (2004).
[18] M. Manga, "Waves of bubbles in basaltic magmas and lavas," J. Geophys. Res. **101**, 457, DOI: 10.1029/95JA02860 (1996).
[19] D. A. Drew, "Mathematical modelling of two-phase flow," Annu. Rev. Fluid Mech. **15**, 261 (1983).
[20] D. A. Drew and S. L. Passman, *Theory of Multicomponent Fluids* (Springer-Verlag, Berlin, 1999).
[21] M. Ishii, *Thermo-Fluid Dynamic Theory of Two-Phase Flow* (Eyrolles, Paris, 1975).
[22] G. K. Batchelor, "A new theory of the instability of a uniform fluidized bed," J. Fluid Mech. **193**, 75 (1988).
[23] J. H. Lammers and A. Biesheuvel, "Concentration waves and the instability of bubbly flow," J. Fluid Mech. **328**, 67 (1996).
[24] A. Biesheuvel and W. C. M. Gorissen, "Void fraction disturbances in uniform bubbly dispersions," Int. J. Multiphase Flow **16**, 211 (1980).
[25] P. E. Lisseter and A. C. Fowler, "Bubbly flow Part II, Modelling void fraction waves," Int. J. Multiphase Flow **18**, 205 (1992).
[26] P. E. Lisseter and A. C. Fowler, "Bubbly flow: I. A simplified model," Int. J. Multiphase Flow **18**, 195 (1992).
[27] C. Pauchon and S. Banerjee, "Interphase momentum interaction effects in the averaged multifield model, Part II: Kinematic waves and interfacial drag in bubbly flow," Int. J. Multiphase Flow **14**, 253 (1988).
[28] A. C. Fowler, *Mathematical Models in the Applied Sciences* (Cambridge University Press, Cambridge, 1997).
[29] D. J. Needham and J. H. Merkin, "On roll waves down an open inclined channel," Proc. R. Soc. London, Ser. A **394**, 259 (1984).
[30] J. J. Stoker, *Water Waves* (Interscience, New York, 1957).
[31] R. F. Dressler, "Mathematical solution of the problem of roll waves in inclined open channels," Commun. Pure Appl. Math. **2**, 149 (1949).
[32] N. J. Balmforth, and S. Mandre, "Dynamics of roll waves," J. Fluid Mech. **514**, 1 (2004).
[33] L. van Wijngaarden and C. Kapteyn, "Concentration waves in dilute bubble/liquid mixtures," J. Fluid Mech. **212**, 111 (1990).
[34] G. B. Whitham, *Linear and Nonlinear Waves* (Wiley-Interscience, New York, 1974).
[35] R. I. Nigmatulin, "Spatial averaging in the mechanics of heterogeneous and dispersed systems," Int. J. Multiphase Flow **5**, 353 (1979).
[36] J. H. Stuhmiller, "The influence of interfacial pressure forces on the character of two-phase flow model equations," Int. J. Multiphase Flow **3**, 551 (1977).
[37] J.-W. Park, D. A. Drew, and R. T. Lahey, Jr., "The analysis of void wave propagation in adiabatic monodispersed bubbly two-phase flows using an ensemble-averaged two-fluid model," Int. J. Multiphase Flow **24**, 1205 (1998).
[38] S.-J. Lee, K.-S. Chang, and K. Kim, "Pressure wave speeds from the characteristics of two fluids, two-phase hyperbolic equation system," Int. J. Multiphase Flow **24**, 855 (1998).
[39] G. B. Wallis, *One-Dimensional Two-Phase Flow* (McGraw-Hill, New York, 1969).
[40] G. K. Batchelor, *An Introduction to Fluid Mechanics* (Cambridge University Press, Cambridge, 1967).